Journal of Nondestructive Evaluation (2020) 39:59
https://doi.org/10.1007/s10921-020-00702-4

A Comparative Study on Structural Damage Detection Using Derivatives of Laser-Measured Flexural and Longitudinal Vibration Shapes

Wei Xu[1,2] · Weidong Zhu[1] · Yongfeng Xu[3] · Maosen Cao[2]

Received: 18 October 2019 / Accepted: 3 July 2020 / Published online: 25 July 2020
© Springer Science+Business Media, LLC, part of Springer Nature 2020

Abstract
Structural damage detection methods relying on laser-measured vibration shapes have become a research focus in the past decade. For damage in a beam/bar with reduced cross-sectional dimensions, such as a notch, it causes changes in both its bending stiffness and axial stiffness in the damage region. Such stiffness changes can induce discontinuities in derivatives of flexural and longitudinal vibration shapes, whereby the damage can be detected and located. Derivatives of flexural vibration shapes have been widely used for structural damage detection, whereas derivatives of longitudinal vibration shapes were recently proposed for structural damage detection and have attracted much less attention. Although it is difficult to excite and measure longitudinal vibration, it can be useful for detecting damage in such a structure as a cable, since flexural vibration of the cable is mainly governed by its tension and not its bending stiffness. In this study, capabilities of derivatives of laser-measured flexural and longitudinal vibration shapes in structural damage detection are comprehensively compared. In particular, to overcome their common deficiency of being susceptible to environmental noise interference, the multiscale analysis based on wavelet transform is integrated into derivatives of vibration shapes to enhance their robustness against noise interference. Analytical and experimental validation shows that compared with commonly used derivatives of flexural vibration shapes, derivatives of longitudinal vibration shapes have the same capability in detecting damage in beam/bar-type structural components.

Keywords Structural damage detection · Derivative of vibration shape · Flexural vibration · Longitudinal vibration · Multiscale analysis · Laser scanning measurement

1 Introduction

Beam/bar-type structural components are important elements in the fields of mechanical, aerospace, and civil engineering. It is of significance to detect damage in beam/bar-type structural components to ensure the integrity and safety of these structures. Structural damage detection methods relying on vibration has attracted increasing attention during the recent decades [1]. Structural vibration shapes (VSs), including mode shapes (MSs) and steady-state response shapes under harmonic excitation (SRSHEs), have been increasingly used for damage detection and localization of structural components [2–6].

For damage in a beam/bar with reduced cross-sectional dimensions, such as a notch, it reduces both its bending stiffness and axial stiffness in the damage region, leading to discontinuities in derivatives of its flexural and longitudinal VSs, respectively. Thereby, the damage can be detected

✉ Weidong Zhu
wzhu@umbc.edu

Wei Xu
wxu@hhu.edu.cn

Yongfeng Xu
xu2yf@uc.edu

Maosen Cao
cmszhy@hhu.edu.cn

[1] Department of Mechanical Engineering, University of Maryland Baltimore County, Baltimore, MD 21250, USA

[2] Department of Engineering Mechanics, Hohai University, Nanjing 210098, China

[3] Department of Mechanical and Materials Engineering, University of Cincinnati, Cincinnati, OH 45221, USA

and located by local discontinuities in derivatives of VSs [7, 8]. For flexural vibration of beams, derivatives of their flexural VSs have been commonly utilized for damage detection because flexural VSs of beams can be easily measured using conventional sensors such as accelerometers and PZT sensors. In contrast, it is much more difficult to measure torsional and longitudinal VSs of beams/bars using conventional sensors. Therefore, most VS-based damage detection methods rely on flexural VSs, such as curvature mode shape (CMS)- [8–16], strain energy- [17–19], pseudo force- [20–22], and wavelet transform-based [23–26] methods. In particular, CMSs, which are the second-order derivatives of flexural MSs, have been widely used for damage detection and localization of beams in the past two decades [8]. Extended from the concept of CMS, a general concept of curvature vibration shape (CVS) can be defined as the second-order derivative of a flexural VS, which can be a MS or a SRSHE. Flexural vibration of beams can be measured through non-contact laser scanning measurement using a scanning laser vibrometer (SLV), whereby flexural VSs with densely distributed measurement points can be obtained. For longitudinal vibration of a beam/bar, the concept of slope vibration shape (SVS), which is the first-order derivatives of a longitudinal VS of the beam/bar, was recently proposed for damage detection and localization of the beam/bar [7]. To measure longitudinal VSs of a beam/bar with densely distributed measurement points, a three-dimensional (3D) SLV with three scanning heads is required to measure its longitudinal vibration. For torsional vibration of a beam, although it can be sensitive to damage [27], it is difficult to excite its torsional vibration and measure its VSs.

For a beam/bar that bears a notch damage, the damage can be detected by its CVSs and SVSs with distinct physical senses. For flexural vibration of a beam, due to the damage-caused change in its bending stiffness, the second-order derivatives of its flexural VSs, i.e., CVSs, become discontinuous at damage edges to balance continuity conditions of bending moments, whereby the damage can be indicated and located by discontinuities in CVSs. For longitudinal vibration of a beam/bar, due to the damage-caused change in its axial stiffness, the first-order derivatives of its longitudinal VSs, i.e., SVSs, become discontinuous at damage edges to balance continuity conditions of axial forces, whereby the damage can be indicated and located by discontinuities in SVSs. Structural damage detection methods relying on CVSs have been widely developed, whereas the method relying on SVSs was recently proposed [7] and has attracted much less attention. While it is much more difficult to excite and measure longitudinal vibration of a beam/bar, and a 3D SLV is required to measure its longitudinal VSs, a longitudinal VS can be useful for detecting damage in such a structure as a cable, since flexural vibration of the cable is mainly governed by its tension and not its bending stiffness. In these cases, SVSs instead of CVSs are suitable to detect damage that causes reduction in elastic modulus and cross-sectional dimensions. By addressing this issue, this comparative study aims to provide a comprehensive comparison between capabilities of methods based on CVSs and SVSs in detecting damage in a beam/bar in aspects of physical senses, analytical formulation, and numerical evaluation. Conclusions from this study can instruct engineers in choosing and using derivatives of flexural and longitudinal VSs for damage detection of beam/bar-type structural components through laser scanning measurement.

It is noteworthy that susceptibility to environmental noise interference is the common deficiency of CVSs and SVSs from densely sampled laser-measured VSs [19]. With this concern, the multiscale analysis based on wavelet transform (WT) is introduced into the CVSs and SVSs in this study, by which novel concepts of multiscale curvature of VS (MCVS) and multiscale slope of VS (MSVS) are formulated to enhance the robustness of the CVSs and SVSs against environmental noise interference.

The rest of this paper is organized as follows. Section 2 introduces fundamentals of the CVSs and SVSs for damage detection of a beam/bar, and reveals mechanisms of generating damage-induced discontinuities of the CVSs and SVSs in respective physical senses. The MCVSs and MSVSs are formulated in Sect. 3 by integrating the WT-based multiscale analysis into the CVSs and SVSs, respectively. Section 4 compares capabilities of the MCVSs and MSVSs in damage detection using flexural and longitudinal VSs of a beam/bar with a two-sided notch, respectively. Experimental validation is conducted in Sect. 5 using a 3D SLV to measure flexural and longitudinal VSs of an aluminum beam with a two-sided notch. Section 6 gives comparison and conclusions of damage detection methods using derivatives of laser-measured flexural and longitudinal VSs.

2 Damage Detection Using Derivatives of Flexural and Longitudinal VSs

2.1 Damage Detection Using CVSs

The bending moment $M(x,t)$ in a beam can be expressed as [28]

$$M(x,t) = E(x)I(x)\frac{\partial^2 w(x,t)}{\partial x^2}, \tag{1}$$

where $w(x,t)$ is the flexural displacement of the beam with x being the spatial coordinate and t being time, $E(x)$ is the elastic modulus, and $I(x)$ is the area moment of inertia of a cross-section. The continuity condition of the bending moment at a position $x = \zeta$ can be written as

$$E(x)I(x)\frac{\partial^2 w(x,t)}{\partial x^2}\bigg|_{x=\zeta^-} = E(x)I(x)\frac{\partial^2 w(x,t)}{\partial x^2}\bigg|_{x=\zeta^+}. \quad (2)$$

For an undamped beam, by assuming $w(x,t) = W_M(x)\sin(\omega_n t)$ with ω_n denoting an undamped flexural natural frequency, the displacement $w(x,t)$ can be expressed as the product of the flexural MS $W_M(x)$ and $\sin(\omega_n t)$. Also, the displacement can be assumed as $w(x,t) = W_S(x)\sin(\omega t)$ with ω denoting an excitation frequency that excludes an undamped flexural natural frequency and $W_S(x)$ being the corresponding flexural SRSHE [28]. Substituting the $w(x,t)$ expression in either case into Eq. (2) yields

$$E(x)I(x)\frac{\mathrm{d}^2 W(x)}{\mathrm{d}x^2}\bigg|_{x=\zeta^-} = E(x)I(x)\frac{\mathrm{d}^2 W(x)}{\mathrm{d}x^2}\bigg|_{x=\zeta^+}, \quad (3)$$

where $W(x)$ is the flexural VS that can be either the flexural MS $W_M(x)$ or the flexural SRSHE $W_S(x)$.

Based on Eq. (3), damage-caused changes in material and/or geometrical parameters $E(x)$ and/or $I(x)$ between $x = \zeta^-$ and $x = \zeta^+$ can cause a discontinuity in $\frac{\mathrm{d}^2 W(x)}{\mathrm{d}x^2}$ between $x = \zeta^-$ and $x = \zeta^+$, which indicates occurrence of damage in the beam. The curvature of $W(x)$, denoted as $CVS(x)$, is written as

$$CVS(x) = \frac{\mathrm{d}^2 W(x)}{\mathrm{d}x^2}, \quad (4)$$

whose discrete form by the second-order central differentiation is

$$CVS(x_k) = \frac{W(x_{k+1}) - 2W(x_k) + W(x_{k-1})}{h^2}, \quad (5)$$

where $k = 2, 3, 4, \ldots, x_k$ denotes the kth spatial sampling point, and h is the sampling interval. In a physical sense, $CVS(x)$ can be a measure of change in the bending stiffness $E(x)I(x)$: by Eq. (3), $M(x)$ is continuous along the beam regardless of damage, and damage-caused change in $E(x)I(x)$ can lead to a discontinuity in $CVS(x)$ at the damage location to balance Eq. (3). Thereby, $CVS(x)$ can be used for indicating and locating damage in the beam.

2.2 Damage Detection Using SVSs

An axial force $F(x,t)$ in a beam/bar can be expressed as [28]

$$F(x,t) = E(x)A(x)\frac{\partial u(x,t)}{\partial x}, \quad (6)$$

where $u(x,t)$ is the longitudinal displacement of the beam/bar and $A(x)$ is the cross-sectional area. The continuity condition of the axial force at a position $x = \zeta$ can be written as

$$E(x)A(x)\frac{\partial u(x,t)}{\partial x}\bigg|_{x=\zeta^-} = E(x)A(x)\frac{\partial u(x,t)}{\partial x}\bigg|_{x=\zeta^+}. \quad (7)$$

By assuming that the beam/bar is undamped, its longitudinal MSs, denoted as $U_M(x)$, can be obtained by assuming $u(x,t) = U_M(x)\sin(\omega_n t)$, where ω_n is an undamped longitudinal natural frequency. One can also assume $u(x,t) = U_S(x)\sin(\omega t)$, where $U_S(x)$ denotes the longitudinal SRSHE at an excitation frequency ω that excludes an undamped longitudinal natural frequency [28]. Substituting the $u(x,t)$ expression in either case into Eq. (7) yields

$$E(x)A(x)\frac{\mathrm{d}U(x)}{\mathrm{d}x}\bigg|_{x=\zeta^-} = E(x)A(x)\frac{\mathrm{d}U(x)}{\mathrm{d}x}\bigg|_{x=\zeta^+}, \quad (8)$$

where $U(x)$ is the longitudinal VS that can be either the longitudinal MS $U_M(x)$ or the longitudinal SRSHE $U_S(x)$.

Based on Eq. (8), damage-caused changes in material and/or geometrical parameters $E(x)$ and/or $A(x)$ between $x = \zeta^-$ and $x = \zeta^+$ can cause a discontinuity in $\frac{\mathrm{d}U(x)}{\mathrm{d}x}$ between $x = \zeta^-$ and $x = \zeta^+$, which indicates occurrence of damage in the beam/bar. The slope of $U(x)$, denoted as $SVS(x)$, is written as

$$SVS(x) = \frac{\mathrm{d}U(x)}{\mathrm{d}x}, \quad (9)$$

whose discrete form by the first-order central differentiation is

$$SVS(x_k) = \frac{U(x_{k+1}) - U(x_{k-1})}{2h}. \quad (10)$$

In a physical sense, $SVS(x)$ can be a measure of change in the axial stiffness $E(x)A(x)$: by Eq. (8), $F(x)$ is continuous along the beam/bar regardless of damage, and damage-caused change in $E(x)A(x)$ can lead to a discontinuity in $SVS(x)$ at the damage location to balance Eq. (8). Thereby, $SVS(x)$ can be used for indicating and locating damage in the beam/bar.

It is noteworthy that both the damage detection methods using the CVSs and SVSs are baseline free. Although flexural and longitudinal VSs depend on boundary conditions, material and geometrical parameters, amplitudes of excitations, etc., prior knowledge of these information can be absent in damage detection.

3 Multiscale Derivatives of Flexural and Longitudinal VSs

As environmental noise can be inevitably involved in laser-measured VSs with dense spatial sampling, noise components in flexural and longitudinal VSs can be largely amplified by differentiation operations in Eqs. (4) and (9), respectively. As a result, actual damage-induced

discontinuities in CVSs and SVSs can be masked by intense noise interference. By addressing this problem, the WT-based multiscale analysis is introduced and integrated into the CVSs and SVSs to formulate the MCVSs and MSVSs for damage detection of beams/bars, respectively.

3.1 Continuous WT

A continuous mother wavelet $\psi(x)$ with a zero mean is defined as [29]

$$\int_{-\infty}^{\infty} \psi(x)\mathrm{d}x = 0, \tag{11}$$

and satisfies the admissibility condition

$$\int_{-\infty}^{\infty} \frac{|\hat{\psi}(\omega)|^2}{\omega}\mathrm{d}\omega < \infty, \tag{12}$$

where $\hat{\psi}(\omega)$ is the Fourier counterpart of $\psi(x)$; $\psi(x)$ is usually normalized in energy:

$$\int_{-\infty}^{\infty} \psi^2(x)\mathrm{d}x = 1. \tag{13}$$

By translating and scaling the mother wavelet $\psi(x)$, a wavelet function $\psi_{v,s}(x)$ is generated [29]:

$$\psi_{v,s}(x) = \frac{1}{\sqrt{s}}\psi\left(\frac{x-v}{s}\right). \tag{14}$$

Accordingly, the continuous WT of a function $f(x)$ can be written as

$$\begin{aligned} Wf(v,s) &= \int_{-\infty}^{\infty} f(x)\psi_{v,s}(x)\mathrm{d}x \\ &= \frac{1}{\sqrt{s}}\int_{-\infty}^{\infty} f(x)\psi\left(\frac{x-v}{s}\right)\mathrm{d}x \\ &= f \otimes \overline{\psi}_s(v), \end{aligned} \tag{15}$$

where $\otimes$ denotes convolution, $\overline{\psi}_s(x) = \frac{1}{\sqrt{s}}\psi\left(\frac{-x}{s}\right)$, v is the translation parameter that describes the location of the window of $\overline{\psi}_s$ sliding along the coordinate x, and s is the scale parameter that describes the width of the window of $\overline{\psi}_s$. Note that $Wf(v,s)$ is a wavelet transform coefficient for given v and s. The continuous WT divides a signal $f(x)$ into continuous levels by the scale parameter s. When scale parameters increase to satisficing levels, noise components can be eliminated; meanwhile damage-induced discontinuities in the MCVSs and MSVSs can be retained [29].

3.2 Novel Concepts of MCVS and MSVS

A family of continuous mother wavelets can be expressed as the nth-order derivative of a function $\theta(x)$ [29]:

$$\psi_n(x) = (-1)^n \frac{\mathrm{d}^n\theta(x)}{\mathrm{d}x^n}. \tag{16}$$

As n specifies that the mother wavelet $\psi_n(x)$ has the nth-order vanishing moment, the WT can be implemented to calculate derivatives of VSs for any given scale parameter. Due to the merits of the Gaussian function $g(x)$ in mathematics, including smoothness, differentiability, localization in the spatial domain, explicit mathematical expressions, and flexibility in manipulation [29], it is used as the function $\theta(x)$ to generate the Gaussian wavelet family in this study:

$$\theta(x) = g(x) = (2/\pi)^{1/4}e^{-x^2}, \tag{17}$$

$$g_n(x) = (-1)^n \frac{\mathrm{d}^n g(x)}{\mathrm{d}x^n}. \tag{18}$$

For the CVSs and SVSs, $g_2(x)$ is an appropriate mother wavelet because of its proper vanishing moment and property of symmetry:

$$MCVS(v,s) = \frac{1}{\sqrt{s}}\int_{-\infty}^{+\infty} CVS(x)g_2\left(\frac{x-v}{s}\right)\mathrm{d}x = \frac{1}{\sqrt{s}}W'' \otimes \overline{g}_{2,s}(v), \tag{19}$$

$$MSVS(v,s) = \frac{1}{\sqrt{s}}\int_{-\infty}^{+\infty} SVS(x)g_2\left(\frac{x-v}{s}\right)\mathrm{d}x = \frac{1}{\sqrt{s}}U' \otimes \overline{g}_{2,s}(v), \tag{20}$$

where $\overline{g}_{2,s} = g_2\left(\frac{-x}{s}\right)$, and $MCVS(v,s)$ and $MSVS(v,s)$ represent the MCVS and MSVS scaled by s at the location of $x = v$, respectively.

By the theorem of convolution differentiation [29], $MCVS(v,s)$ and $MSVS(v,s)$ can be written as

$$MCVS(v,s) = \frac{1}{\sqrt{s}}W'' \otimes \overline{g}_{2,s}(v) = \frac{1}{\sqrt{s}}W \otimes \overline{g}''_{2,s}(v), \tag{21}$$

$$MSVS(v,s) = \frac{1}{\sqrt{s}}U' \otimes \overline{g}_{2,s}(v) = \frac{1}{\sqrt{s}}U \otimes \overline{g}'_{2,s}(v). \tag{22}$$

By Eqs. (21) and (22), $MCVS(v,s)$ and $MSVS(v,s)$ are further written as

$$MCVS(v,s) = \frac{1}{\sqrt{s}}W \otimes \overline{g}''_{2,s}(v) = \frac{1}{s^{5/2}}\int_{-\infty}^{+\infty} W(x)g_4\left(\frac{x-v}{s}\right)\mathrm{d}x, \tag{23}$$

$$MSVS(v,s) = \frac{1}{\sqrt{s}}U \otimes \overline{g}'_{2,s}(v) = -\frac{1}{s^{3/2}}\int_{-\infty}^{+\infty} U(x)g_3\left(\frac{x-v}{s}\right)\mathrm{d}x, \tag{24}$$

where $g_3(x) = \frac{1}{\sqrt{15}}(2/\pi)^{1/4}(12x - 8x^3)e^{-x^2}$ is the third-order Gaussian wavelet and $g_4(x) = \frac{1}{\sqrt{105}}(2/\pi)^{1/4}(12 - 48x^2 + 16x^4)e^{-x^2}$ is the fourth-order Gaussian wavelet.

Equations (23) and (24) produce novel concepts of MCVS and MSVS, respectively, which exhibit the intrinsic multiscale property of WT. The merits of the multiscale analysis integrated into the CVSs and SVSs are twofold. By gradually increasing the scale parameters to satisficing levels, noise components in the MCVSs and MSVSs can be gradually eliminated; meanwhile the damage-induced discontinuities can be retained for indicating and locating the damage. On the other hand, the physical senses of the CVSs and SVSs are retained in the MCVSs and MSVSs, respectively. As the MCVSs and MSVSs are developed from the CVSs and SVSs, respectively, naturally, their respective mechanisms of generating damage-induced discontinuities are retained, as expressed in Eqs. (3) and (8).

4 Analytical Investigation

4.1 Analytical Formulation of Flexural and Longitudinal VSs

Consider an undamped beam/bar of length L, which contains a notch along its length. The beam/bar is divided into three segments by edges of the notch section with lengths L_j ($j = 1, 2, 3$). Two intact segments are joined by the notch segment with reduced cross-sectional dimensions. Let x_j be the abscissa of the jth change in the cross-section and $l_j = x_j/L$ be the dimensionless abscissa of x_j. The elastic modulus and material density of the beam/bar are denoted as E and ρ, respectively. The cross-sectional area and area moment of inertia of the jth segment are A_j and I_j, respectively. It is noteworthy that although numerical methods such as the finite element method can be used to model the damaged beam/bar and calculate its VSs, analytical formulation of the VSs is in accord with the physical senses of the CVSs and SVSs in Eqs. (3) and (8), respectively, in its damage detection.

4.1.1 Analytical Formulation of Flexural MSs

The equation of flexural motion of the jth segment of the undamped beam is expressed as [30]

$$EI_j\frac{\partial^4 w_j}{\partial x^4} + \rho A_j\frac{\partial^2 w_j}{\partial t^2} = 0, \quad j = 1, 2, 3, \tag{25}$$

where w_j is the flexural displacement of the jth segment, whose solution can be assumed as

$$w_j(x, t) = W_{M,j}(x)\sin(\omega_n t), \tag{26}$$

where $W_{M,j}(x)$ is the jth segment of the flexural MS associated with the natural frequency ω_n. Substituting Eq. (26) into Eq. (25) yields

$$\frac{\mathrm{d}^4 W_{M,j}}{\mathrm{d}x^4} - \frac{\rho A_j}{EI_j}\omega_n^2 W_{M,j} = 0. \tag{27}$$

By introducing the dimensionless abscissa $\zeta = x/L$, the general solution to Eq. (27) can be expressed as

$$\begin{aligned}
W_{M,1}(\zeta) &= a_{M,1}\cos\lambda_{M,1}\zeta + b_{M,1}\sin\lambda_{M,1}\zeta + c_{M,1}\cosh\lambda_{M,1}\zeta \\
&\quad + d_{M,1}\sinh\lambda_{M,1}\zeta, \quad 0 \le \zeta \le l_1, \\
W_{M,2}(\zeta) &= a_{M,2}\cos\lambda_{M,2}\zeta + b_{M,2}\sin\lambda_{M,2}\zeta + c_{M,2}\cosh\lambda_{M,2}\zeta \\
&\quad + d_{M,2}\sinh\lambda_{M,2}\zeta, \quad l_1 \le \zeta \le l_2, \\
W_{M,3}(\zeta) &= a_{M,3}\cos\lambda_{M,3}\zeta + b_{M,3}\sin\lambda_{M,3}\zeta + c_{M,3}\cosh\lambda_{M,3}\zeta \\
&\quad + d_{M,3}\sinh\lambda_{M,3}\zeta, \quad l_2 \le \zeta \le 1,
\end{aligned} \tag{28}$$

where $a_{M,j}$, $b_{M,j}$, $c_{M,j}$, and $d_{M,j}$, in which $j = 1,2,3$, are constants to be determined by boundary and continuity conditions, and $\lambda_{M,j} = L\sqrt[4]{\omega_n^2\rho A_j/EI_j}$ is the dimensionless natural frequency of each beam segment. The slope of the transverse displacement, bending moment, and shear force are expressed as $W'_{M,j}(\zeta)$, $EIW''_{M,j}(\zeta)$, and $EIW'''_{M,j}(\zeta)$, respectively.

By taking a cantilever beam as an example, its boundary conditions at its two ends are

$$\begin{aligned}
&W_{M,1}(\zeta)\big|_{\zeta=0} = 0, \quad W'_{M,1}(\zeta)\big|_{\zeta=0} = 0, \\
&W''_{M,3}(\zeta)\big|_{\zeta=1} = 0, \quad W'''_{M,3}(\zeta)\big|_{\zeta=1} = 0.
\end{aligned} \tag{29}$$

Continuity conditions of the displacement, slope, bending moment, and shear force at two edges of the notch section, i.e., $\zeta = l_1$ and $\zeta = l_2$, are

$$\begin{aligned}
&W_{M,1}(\zeta) = W_{M,2}(\zeta)\big|_{\zeta=l_1}, \; W'_{M,1}(\zeta) = W'_{M,2}(\zeta)\big|_{\zeta=l_1}, \\
&EI_1W''_{M,1}(\zeta) = EI_2W''_{M,2}(\zeta)\big|_{\zeta=l_1}, \; EI_1W'''_{M,1}(\zeta) = EI_2W'''_{M,2}(\zeta)\big|_{\zeta=l_1};
\end{aligned} \tag{30}$$

and

$$\begin{aligned}
&W_{M,2}(\zeta) = W_{M,3}(\zeta)\big|_{\zeta=l_2}, \; W'_{M,2}(\zeta) = W'_{M,3}(\zeta)\big|_{\zeta=l_2}, \\
&EI_2W''_{M,2}(\zeta) = EI_3W''_{M,3}(\zeta)\big|_{\zeta=l_2}, \; EI_2W'''_{M,2}(\zeta) = EI_3W'''_{M,3}(\zeta)\big|_{\zeta=l_2}.
\end{aligned} \tag{31}$$

Substituting Eq. (28) into Eqs. (29)–(31) yields 12 homogeneous equations with 12 unknown constants $a_{M,j}$, $b_{M,j}$, $c_{M,j}$, and $d_{M,j}$. To obtain a nontrivial solution, the determinant of the coefficient matrix is set to zero, whereby the natural frequencies can be solved and $a_{M,j}$, $b_{M,j}$, $c_{M,j}$, and $d_{M,j}$ can be solved by normalizing mode shapes with unit maximum

absolute values. Accordingly, $W_j(\zeta)$ can be obtained by Eq. (28).

4.1.2 Analytical Solution to Flexural SRSHEs

The equation of flexural motion of the jth segment of the undamped beam under the flexural harmonic excitation $f(x,t)$ at an excitation frequency ω that excludes an umdamped flexural natural frequency is expressed as [30]

$$EI_j\frac{\partial^4 w_j}{\partial x^4}+\rho A_j\frac{\partial^2 w_j}{\partial t^2}=f,\quad j=1,2,3, \tag{32}$$

whose solution can be assumed as

$$w_j(x,t)=W_{S,j}(x)\sin(\omega t), \tag{33}$$

where $W_{S,j}(x)$ is the jth segment of the flexural SRSHE associated with the excitation frequency ω.

Consider a pointwise harmonic excitation $f(x,t)=F\sin(\omega t)\delta(L-x)$ with the amplitude F applied at the free end ($x=L$) of the cantilever beam, where $\delta(\bullet)$ denotes the Dirac delta function. Since $f(x,t)$ vanishes for $x\in[0,L)$, solutions to $W_{S,j}(x)$ for $x\in[0,L)$ have the same forms as those in Eq. (28):

$$\begin{aligned}
W_{S,1}(\zeta)&=a_{S,1}\cos\lambda_{S,1}\zeta+b_{S,1}\sin\lambda_{S,1}\zeta+c_{S,1}\cosh\lambda_{S,1}\zeta+d_{S,1}\sinh\lambda_{S,1}\zeta,0\le\zeta\le l_1,\\
W_{S,2}(\zeta)&=a_{S,2}\cos\lambda_{S,2}\zeta+b_{S,2}\sin\lambda_{S,2}\zeta+c_{S,2}\cosh\lambda_{S,2}\zeta+d_{S,2}\sinh\lambda_{S,2}\zeta,l_1\le\zeta\le l_2,\\
W_{S,3}(\zeta)&=a_{S,3}\cos\lambda_{S,3}\zeta+b_{S,3}\sin\lambda_{S,3}\zeta+c_{S,3}\cosh\lambda_{S,3}\zeta+d_{S,3}\sinh\lambda_{S,3}\zeta,l_2\le\zeta<1,
\end{aligned} \tag{34}$$

where $a_{S,j}$, $b_{S,j}$, $c_{S,j}$, and $d_{S,j}$, in which $j=1,2,3$, are constants to be determined by boundary and continuity conditions, and $\lambda_{S,j}=L\sqrt[4]{\omega^2\rho A_j/EI_j}$ is the dimensionless frequency of each beam segment corresponding to the excitation frequency. The slope of the transverse displacement, bending moment, and shear force are expressed as $W'_{S,j}(\zeta)$, $EIW''_{S,j}(\zeta)$, and $EIW'''_{S,j}(\zeta)$, respectively.

Boundary conditions of the cantilever beam can be expressed as

$$\begin{aligned}
&W_{S,1}(\zeta)\big|_{\zeta=0}=0,\quad W'_{S,1}(\zeta)\big|_{\zeta=0}=0,\\
&W''_{S,3}(\zeta)\big|_{\zeta=1}=0,\quad W'''_{S,3}(\zeta)\big|_{\zeta=1}=-\frac{F}{EI_3}.
\end{aligned} \tag{35}$$

Continuity conditions of the displacement, slope, bending moment, and shear force at two edges of the notch section, i.e., $\zeta=l_1$ and $\zeta=l_2$, are

$$\begin{aligned}
&W_{S,1}(\zeta)=W_{S,2}(\zeta)\big|_{\zeta=l_1},\ W'_{S,1}(\zeta)=W'_{S,2}(\zeta)\big|_{\zeta=l_1},\\
&EI_1W''_{S,1}(\zeta)=EI_2W''_{S,2}(\zeta)\big|_{\zeta=l_1},\ EI_1W'''_{S,1}(\zeta)=EI_2W'''_{S,2}(\zeta)\big|_{\zeta=l_1};
\end{aligned} \tag{36}$$

and

$$\begin{aligned}
&W_{S,2}(\zeta)=W_{S,3}(\zeta)\big|_{\zeta=l_2},\ W'_{S,2}(\zeta)=W'_{S,3}(\zeta)\big|_{\zeta=l_2},\\
&EI_2W''_{S,2}(\zeta)=EI_3W''_{S,3}(\zeta)\big|_{\zeta=l_2},\ EI_2W'''_{S,2}(\zeta)=EI_3W'''_{S,3}(\zeta)\big|_{\zeta=l_2}.
\end{aligned} \tag{37}$$

Substituting Eq. (34) into Eqs. (35)–(37) yields 12 nonhomogeneous equations, from which 12 unknown constants $a_{S,j}$, $b_{S,j}$, $c_{S,j}$, and $d_{S,j}$ can be solved by assuming that the force has a unit amplitude (1 N). Accordingly, $u_{S,j}(\zeta)$ can be obtained from Eq. (34), which has the same shape subject to different force amplitudes under the linear vibration assumption.

4.1.3 Analytical Formulation of Longitudinal MSs

The equation of longitudinal motion of the undamped beam/bar is expressed as [30]

$$E\frac{\partial^2 u_j}{\partial x^2}-\rho\frac{\partial^2 u_j}{\partial t^2}=0,\quad j=1,2,3, \tag{38}$$

where u_j is the longitudinal displacement of the jth segment, whose solution can be assumed as

$$u_j(x,t)=U_{M,j}(x)\sin(\omega_n t),\quad j=1,2,3, \tag{39}$$

where $U_{M,j}(x)$ is the jth segment of the longitudinal MS associated with the natural frequency ω_n. Substituting Eq. (39) into Eq. (38) yields

$$\frac{\mathrm{d}^2U_j}{\mathrm{d}x^2}-\frac{\rho}{E}\omega_n^2U_j=0. \tag{40}$$

By introducing the dimensionless abscissa $\zeta=x/L$, the general solution to Eq. (40) can be expressed as

$$\begin{aligned}
U_{M,1}(\zeta)&=e_{M,1}\cos\eta_{M,1}\zeta+f_{M,1}\sin\eta_{M,1}\zeta,0\le\zeta\le l_1,\\
U_{M,2}(\zeta)&=e_{M,2}\cos\eta_{M,2}\zeta+f_{M,2}\sin\eta_{M,2}\zeta,l_1\le\zeta\le l_2,\\
U_{M,3}(\zeta)&=e_{M,3}\cos\eta_{M,3}\zeta+f_{M,3}\sin\eta_{M,3}\zeta,l_2\le\zeta\le 1,
\end{aligned} \tag{41}$$

where $e_{M,j}$ and $f_{M,j}$, in which $j=1,2,3$, are constants to be determined by boundary and continuity conditions, and $\eta_{M,j}=L\omega_n\sqrt{\rho_j/E_j}$ is the dimensionless natural frequency of each beam/bar segment. The axial force in a beam/bar segment is $EA_jU'_{M,j}(\zeta)$.

By taking a free-free beam/bar as an example, its boundary conditions at its two ends are

$$U'_{M,1}(\zeta)\Big|_{\zeta=0} = 0, \quad U'_{M,3}(\zeta)\Big|_{\zeta=1} = 0 \tag{42}$$

Continuity conditions of the displacement and axial force at two edges of the notch section, i.e., $\zeta = l_1$ and $\zeta = l_2$, are

$$U_{M,1}(\zeta) = U_{M,2}(\zeta)\Big|_{\zeta=l_1}, \quad EA_1 U'_{M,1}(\zeta) = EA_2 U'_{M,2}(\zeta)\Big|_{\zeta=l_1}; \tag{43}$$

and

$$U_{M,2}(\zeta) = U_{M,3}(\zeta)\Big|_{\zeta=l_2}, \quad EA_2 U'_{M,2}(\zeta) = EA_3 U'_{M,3}(\zeta)\Big|_{\zeta=l_2}. \tag{44}$$

Substituting Eq. (41) into Eqs. (42)–(44) yields six homogeneous equations with six unknown constants $e_{M,j}$ and $f_{M,j}$. To obtain a nontrivial solution, the determinant of the coefficient matrix is set to zero, from which the natural frequencies can be solved and $e_{M,j}$ and $f_{M,j}$ can be solved by normalizing mode shapes with unit maximum absolute values. Accordingly, $U_{M,j}(\zeta)$ can be obtained by Eq. (41).

4.1.4 Analytical Formulation of Longitudinal SRSHEs

The equation of longitudinal motion of the jth segment of the undamped beam/bar under the longitudinal harmonic excitation force $f(x,t)$ at the excitation frequency ω that excludes an undamped longitudinal natural frequency can be assumed as [30]

$$E\frac{\partial^2 u_j}{\partial x^2} - \rho\frac{\partial^4 u_j}{\partial t^2} = f, \quad j = 1,2,3, \tag{45}$$

whose solution can be assumed as

$$u_j(x,t) = U_{S,j}(x)\sin(\omega t), \tag{46}$$

where $U_{S,j}(x)$ is the jth segment of the longitudinal SRSHE associated with the excitation frequency ω.

Consider a pointwise harmonic excitation $f(x,t) = F\sin(\omega t)\delta(L-x)$ with the amplitude F applied at one free end ($x = L$) of the bar. Since $f(x,t)$ vanishes for $x \in [0,L)$, solutions to $U_{S,j}(x)$ for $x \in [0,L)$ have the same forms as those in Eq. (41):

$$\begin{aligned} U_{S,1}(\zeta) &= e_{S,1}\cos\eta_{S,1}\zeta + f_{S,1}\sin\eta_{S,1}\zeta, 0 \le \zeta \le l_1, \\ U_{S,2}(\zeta) &= e_{S,2}\cos\eta_{S,2}\zeta + f_{S,2}\sin\eta_{S,2}\zeta, l_1 \le \zeta \le l_2, \\ U_{S,3}(\zeta) &= e_{S,3}\cos\eta_{S,3}\zeta + f_{S,3}\sin\eta_{S,3}\zeta, l_2 \le \zeta < 1, \end{aligned} \tag{47}$$

where $e_{S,j}$ and $f_{S,j}$, in which $j = 1,2,3$, are constants to be determined by boundary and continuity conditions, and $\eta_{S,j} = L\omega\sqrt{\rho_j/E_j}$ is the dimensionless frequency of each beam/bar segment corresponding to the excitation frequency. The axial force in a beam/bar segment is $EA_j U'_{S,j}(\zeta)$.

Boundary conditions of the free-free beam/bar are

$$U'_{S,3}(\zeta)\Big|_{\zeta=0} = 0, \quad U'_{S,3}(\zeta)\Big|_{\zeta=1} = -\frac{F}{EA_3}. \tag{48}$$

Continuity conditions of the displacement and axial force at two edges of the notch section, i.e., $\zeta = l_1$ and $\zeta = l_2$, are

$$U_{S,1}(\zeta) = U_{S,2}(\zeta)\Big|_{\zeta=l_1}, \quad EA_1 U'_{S,1}(\zeta) = EA_2 U'_{S,2}(\zeta)\Big|_{\zeta=l_1}; \tag{49}$$

and

$$U_{S,2}(\zeta) = U_{S,3}(\zeta)\Big|_{\zeta=l_2}, \quad EA_2 U'_{S,2}(\zeta) = EA_3 U'_{S,3}(\zeta)\Big|_{\zeta=l_2}. \tag{50}$$

Substituting Eq. (47) into Eqs. (48)–(50) yields six nonhomogeneous equations, from which six unknown constants $e_{S,j}$ and $f_{S,j}$ can be solved by assuming that the force has a unit amplitude (1 N). Accordingly, $U_{S,j}(\zeta)$ can be obtained by Eq. (47), which has the same shape subject to different force amplitudes under the linear vibration assumption.

4.2 Damage Detection Results

An aluminum beam/bar of length 45 cm, width 2.5 cm, and thickness 0.6 cm is considered as a specimen, whose elastic modulus and density are 70 GPa and 2700 kg/m^3, respectively. A two-sided notch with reduced cross-sectional dimensions is introduced by reducing 10% of thickness from both top and bottom surfaces of the specimen, spanning from $x = 15$ to 20 cm, i.e., from $\zeta = 0.33$ to 0.44 in the dimensionless coordinate. It is noteworthy that for comparison of damage detection methods relying on MSs and SRSHEs, excitation frequencies are chosen to be close to natural frequencies, and the SRSHEs are close to the corresponding mode shapes [20].

4.2.1 Damage Detection Relying on Flexural VSs

For flexural vibration, the fifth flexural MS at 1330.4 Hz with a unit maximum absolute value is arbitrarily selected and obtained by Eq. (28), whose constants are solved as

$$(\lambda_{M,1}, \lambda_{M,2}, \lambda_{M,3}) = (13.8544, 15.4897, 13.8544),$$

$$\begin{aligned} (a_{M,1}, b_{M,1}, c_{M,1}, d_{M,1}) &= (-0.4962, 0.4984, 0.4962, -0.4984), \\ (a_{M,2}, b_{M,2}, c_{M,2}, d_{M,2}) &= (-0.7695, 0.2341, -1.1189, 1.1189), \\ (a_{M,3}, b_{M,3}, c_{M,3}, d_{M,3}) &= (-0.3408, 0.6197, -51.2012, 51.2012). \end{aligned}$$

By Eq. (34), the flexural SRSHE is produced by the flexural harmonic excitation at 1320 Hz with a unit excitation amplitude, whose constants are solved as

$(\lambda_{S,1}, \lambda_{S,2}, \lambda_{S,3}) = (13.7967, 15.4252, 13.7967)$,

$(a_{S,1}, b_{S,1}, c_{S,1}, d_{S,1}) = (-0.8636, 0.8675, 0.8636, -0.8675) \times 10^{-4}$,

$(a_{S,2}, b_{S,2}, c_{S,2}, d_{S,2}) = (-1.3364, 0.4080, -2.6129, 2.6129) \times 10^{-4}$,

$(a_{S,3}, b_{S,3}, c_{S,3}, d_{S,3}) = (-0.5906, 1.0740, -87.2303, 87.2303) \times 10^{-4}$.

Both the flexural MS and SRSHE are discretized with 251 uniformly distributed sampling points.

Figure 1a and b show the flexural MS and SRSHE, respectively. It can be seen from Fig. 1 that the MS and SRSHE have similar shapes because the natural frequency associated with the MS is close to the excitation frequency for the SRSHE. The CVSs for the MS and SRSHE are obtained by Eq. (5) and shown in Fig. 2a and b, respectively. It can be seen that there are evident discontinuities at $\zeta = 0.33$ and $\zeta = 0.44$, which correspond to the two edges of the notch. To simulate a noisy condition, white Gaussian noise of signal-to-noise ratio (SNR) of 70 dB is individually added to the flexural MS and SRSHE. It can be seen from Fig. 3a and b that noise interference dominates CVSs and masks the damage-induced discontinuities. To eliminate noise interference, MCVSs are obtained by Eq. (23) and shown in Figs. 4a and 5a. In either MCVS, amplitudes of two pairs of singularity peaks and valleys that increase with the scale parameter s clearly indicate locations of the two edges of the notch; either edge lies in the middle of a pair of neighboring peak and valley, reflecting the corresponding discontinuity in the CVS. In Figs. 4b and 5b, the top views of the MCVSs in the v-s plane clearly pinpoint the damage: the detected notch spans from $\zeta = 0.33$ to 0.44, which corresponds to the actual location of the notch whose edges are marked by two dashed lines.

4.2.2 Damage Detection Relying on Longitudinal VSs

As longitudinal natural frequencies are much higher than flexural natural frequencies, the first longitudinal MS associated with the first natural frequency of 5538.3 Hz is considered. The first longitudinal MS is obtained by Eq. (41) and normalized with a unit maximum absolute value, whose constants are solved as

$(\eta_{M,1}, \eta_{M,2}, \eta_{M,3}) = (3.0754, 3.0754, 3.0754)$,

$(e_{M,1}, f_{M,1}) = (2.7244, 0.0000) \times 10^{-6}$,

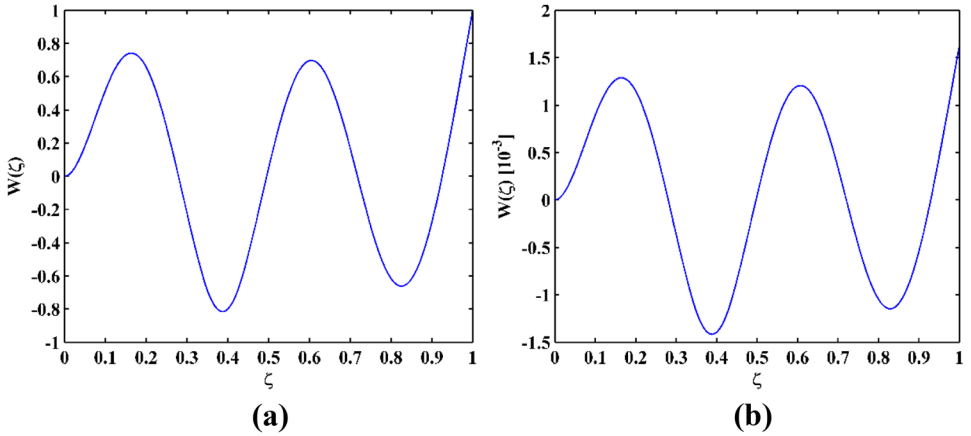

Fig. 1 Noise-free flexural **a** MS at 1330.4 Hz and **b** SRSHE at 1320 Hz

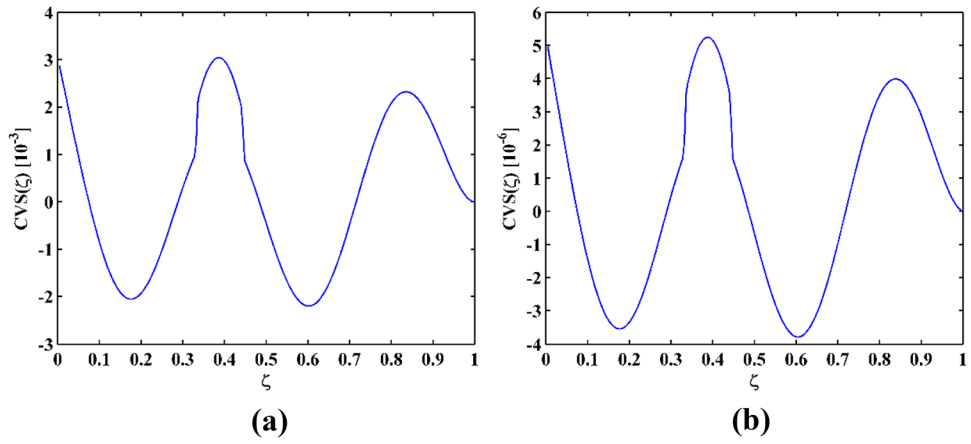

Fig. 2 CVSs for the noise-free flexural **a** MS at 1330.4 Hz and **b** SRSHE at 1320 Hz

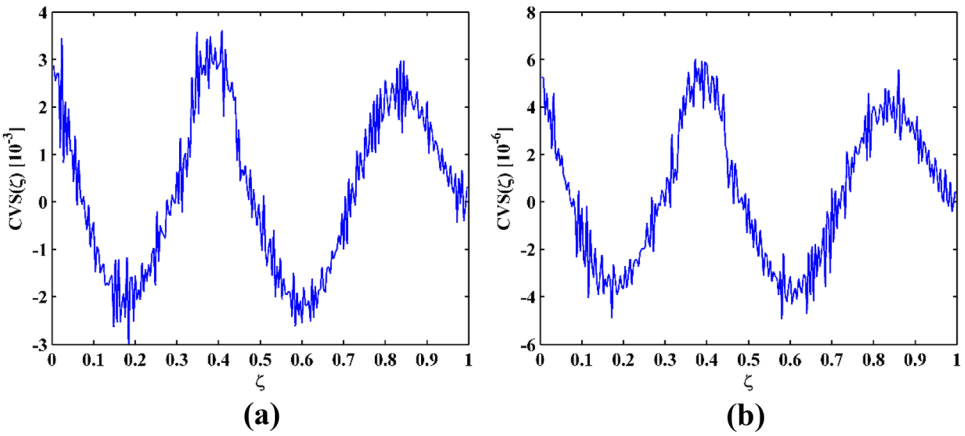

Fig. 3 CVSs for the noisy flexural **a** MS at 1330.4 Hz and **b** SRSHE at 1320 Hz

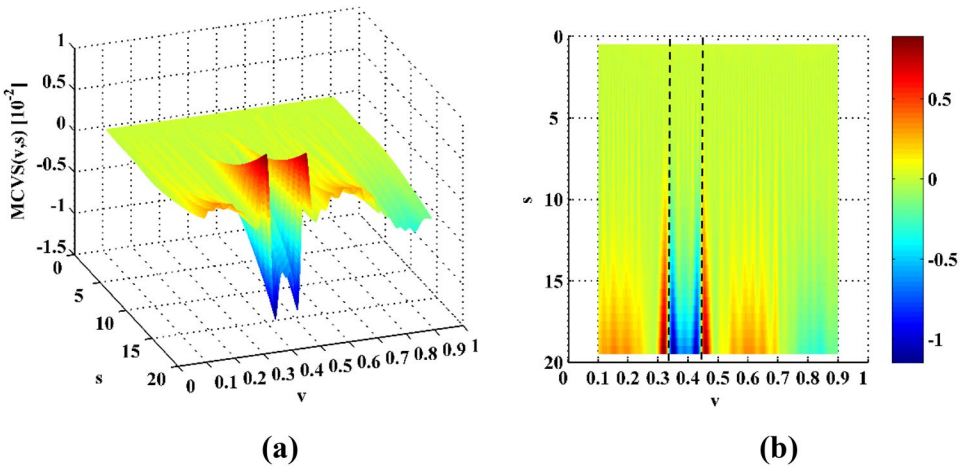

Fig. 4 **a** MCVS for the flexural MS at 1330.4 Hz and **b** its top view

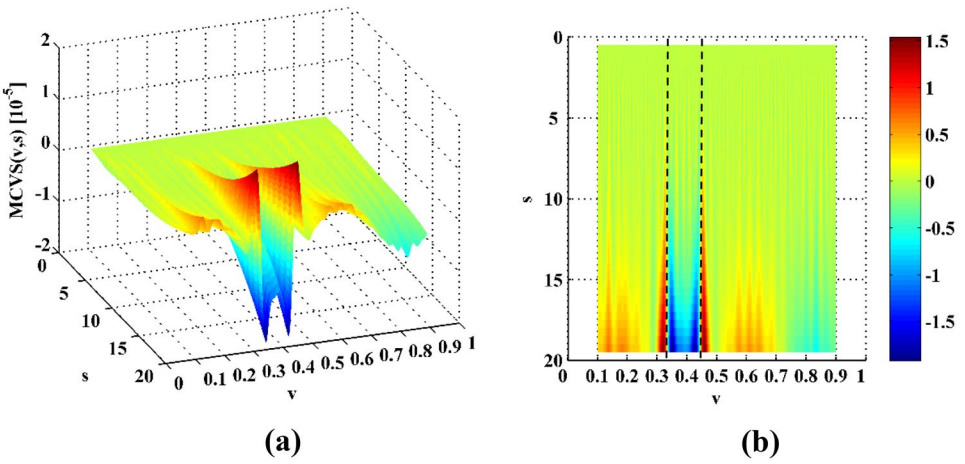

Fig. 5 **a** MCVS for the flexural SRSHE at 1320 Hz and **b** its top view

$$(e_{M,2}, f_{M,2}) = (3.1423, -0.3316) \times 10^{-6},$$

$$(e_{M,3}, f_{M,3}) = (2.5740, -0.1107) \times 10^{-6}.$$

By Eq. (47), the longitudinal SRSHE is produced by the longitudinal harmonic excitation at 4860 Hz with a unit excitation amplitude, whose constants are solved as

$$(\eta_{S,1}, \eta_{S,2}, \eta_{S,3}) = (2.7000, 2.7000, 2.7000),$$

$(e_{S,1}, f_{S,1}) = (1.0000, 0.0000)$,

$(e_{S,2}, f_{S,2}) = (1.1827, -0.1109)$,

$(e_{S,3}, f_{S,3}) = (0.9514, -0.0631)$.

The first longitudinal MS at 5538.3 Hz and longitudinal SRSHE at 4860 Hz are shown in Fig. 6a and b, respectively. SVSs for the MS and SRSHE are obtained by Eq. (10) and shown in Fig. 7a and b, respectively. Similar to CVSs in Fig. 2, it can be seen from Fig. 7 that there are evident discontinuities at $\zeta = 0.33$ and $\zeta = 0.44$, which correspond to the two edges of the notch. For the noisy longitudinal MS and SRSHE with SNR of 70 dB, it can be seen from their respective SVSs in Fig. 8a and b that noise interference dominates and masks the discontinuities induced by the damage. Corresponding MSVSs are obtained by Eq. (24) and shown in Figs. 9a and 10a, respectively; in either figure amplitudes of two pairs of singularity peaks and valleys that increase with the scale parameter s indicate locations of the two edges of the notch. To clearly show the location of the detected notch, the top views of MSVSs are demonstrated in Figs. 9b and 10b, in either of which amplitudes of two pairs of neighboring peaks and valleys appear to reflect the corresponding discontinuities induced by the damage. Hereby, the damage can be clearly detected and located, spanning from $\zeta = 0.33$ to 0.44, which corresponds to the actual location of the notch indicated between two dashed lines.

4.2.3 Feasibility for Low Excitation Frequencies and Small Damage

In reality, fundamental MSs and SRSHEs at low excitation frequencies can be more easily obtained. To verify the feasibility to use SRSHEs associated with low excitation frequencies, especially those that are lower than fundamental natural frequencies, the flexural and longitudinal harmonic excitations are selected to be at half of the flexural and longitudinal fundamental natural frequencies, respectively. On the other hand, to verify the capability of the MCVSs and MSVSs in detecting damage with a smaller extent, only 5% thickness reduction from both top and bottom surfaces of the beam/bar is considered. Noisy flexural and longitudinal SRSHEs associated with excitation frequencies that are half of the flexural and longitudinal fundamental natural

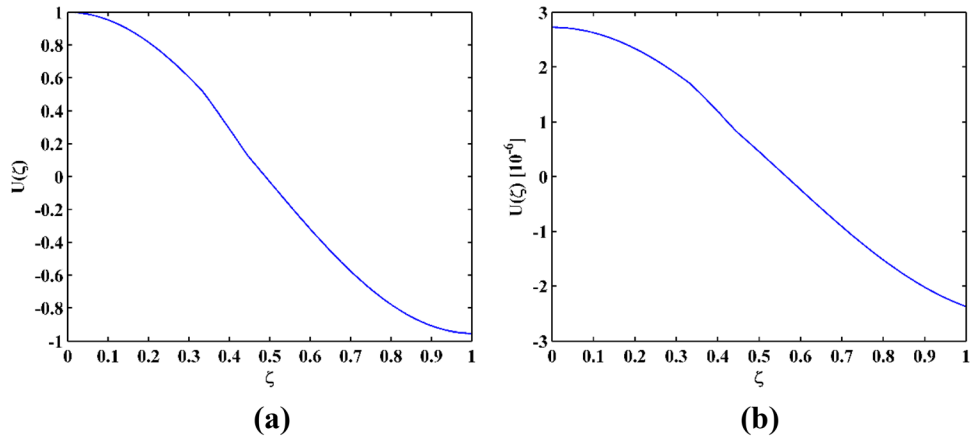

Fig. 6 Noise-free longitudinal **a** MS at 5538.3 Hz and **b** SRSHE at 4860 Hz

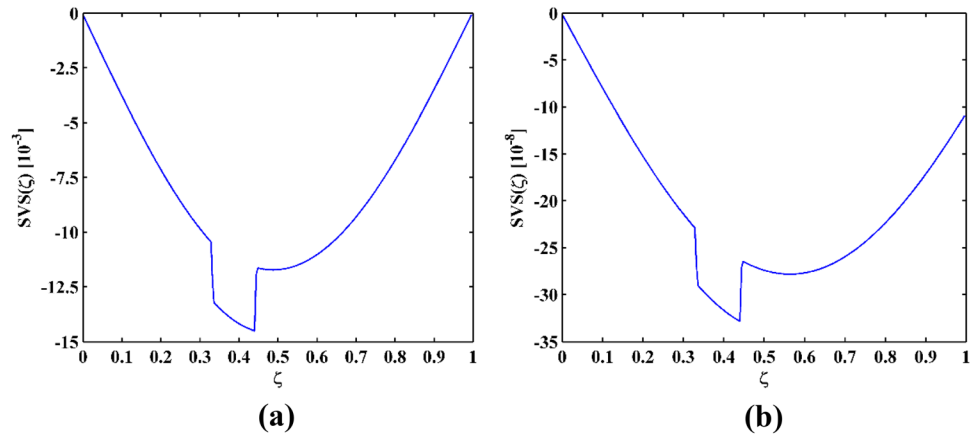

Fig. 7 SVSs for the noise-free longitudinal **a** MS at 5538.3 Hz and **b** SRSHE at 4860 Hz

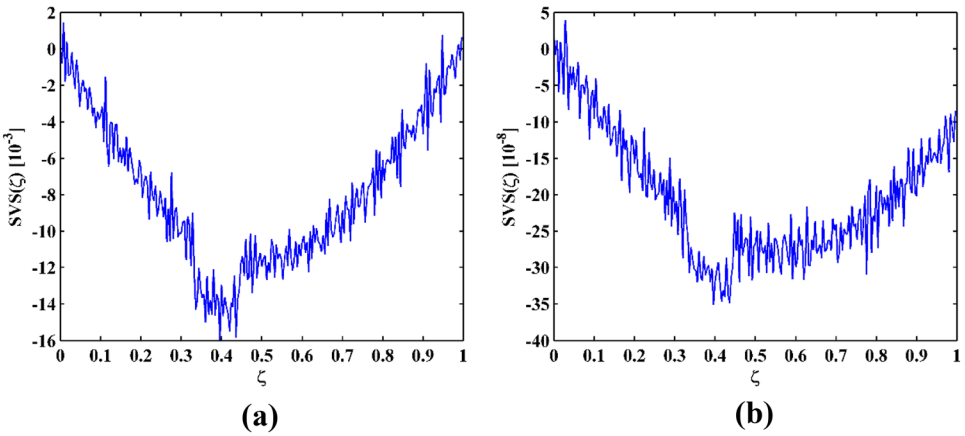

Fig. 8 SVSs for the noisy longitudinal **a** MS at 5538.3 Hz and **b** SRSHE at 4860 Hz

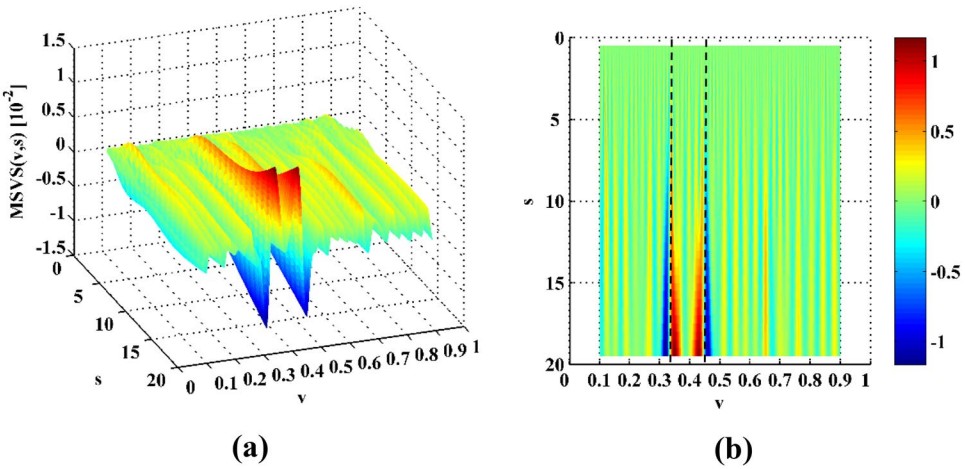

Fig. 9 **a** MSVS for the longitudinal MS at 5538.3 Hz and **b** its top view

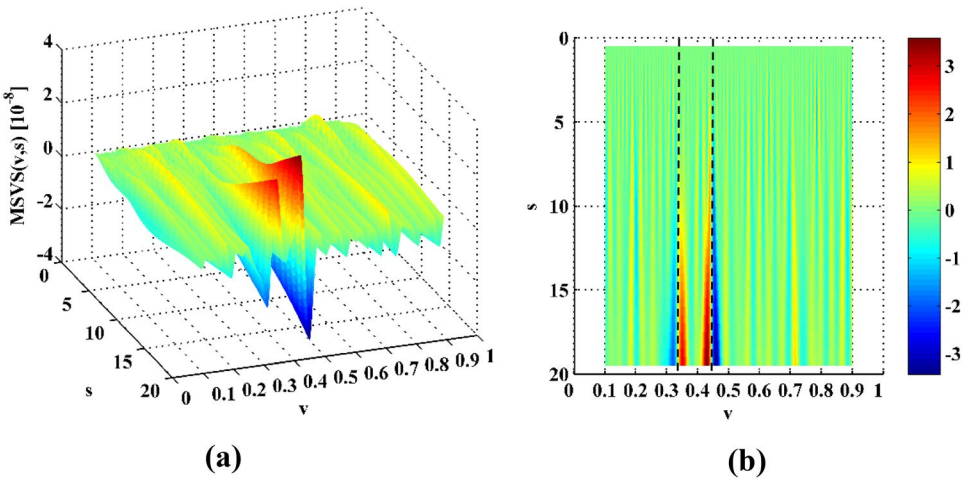

Fig. 10 **a** MSVS for the longitudinal SRSHE at 4860 Hz and **b** its top view

frequencies are shown in Fig. 11a and b, respectively. By Eqs. (23) and (24), the corresponding MCVS and MSVS are obtained and shown in Fig. 12a and c, respectively, where the two edges of the notch with the smaller extent can still be evidently identified. In their top views shown in Fig. 12b and d, neighboring peaks and valleys clearly locate the two edges of the notch, which are in good agreement with the actual edges of the notch that are indicated by dashed lines.

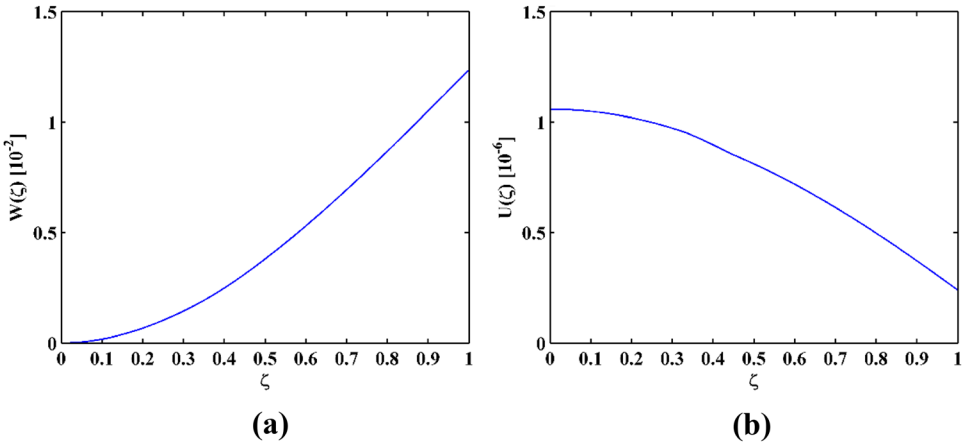

Fig. 11 Noisy **a** flexural and **b** longitudinal SRSHEs at excitation frequencies that are half of the flexural and longitudinal fundamental natural frequencies, respectively

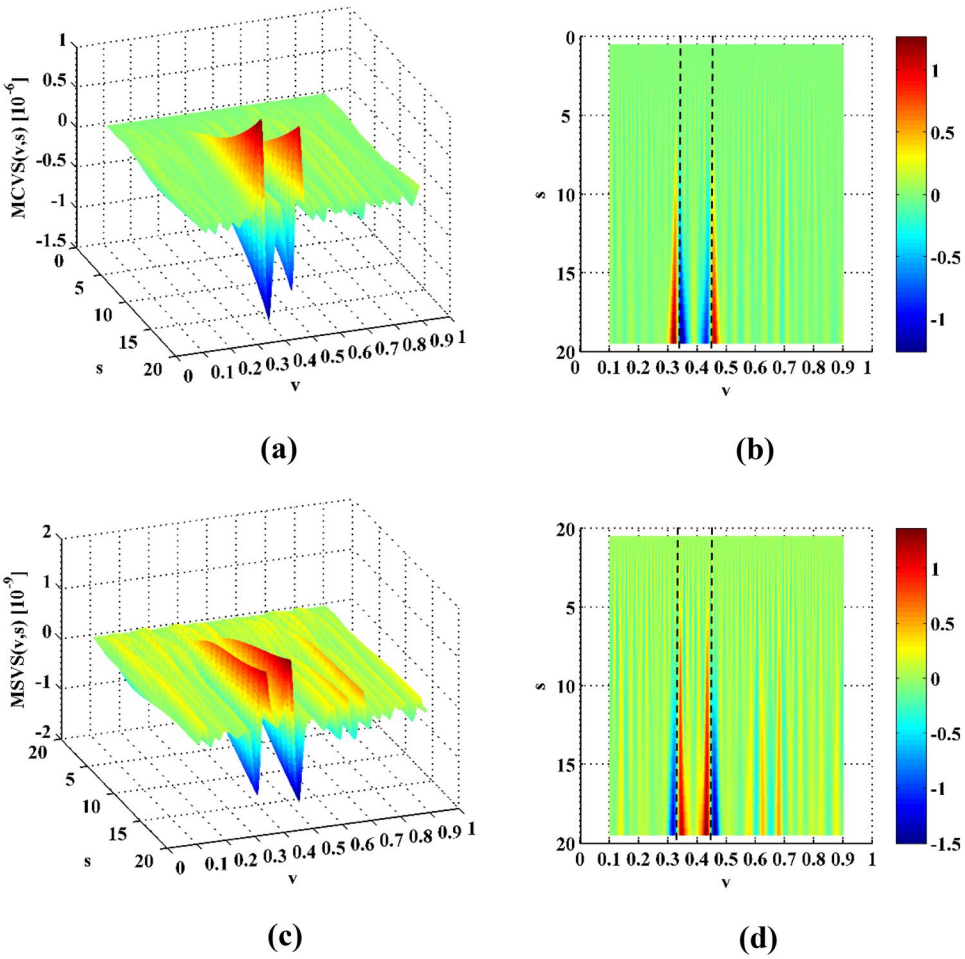

Fig. 12 **a** MCVS and **c** the MSVS, and **b** and **d** their respective top views

5 Experimental Validation

5.1 Experimental Set-Up

The capabilities of the MCVSs and MSVSs in detecting structural damage is experimentally validated on an aluminum beam specimen through laser scanning measurement using a 3D SLV (Polytec PSV-500-3D), as shown in Fig. 13. The specimen is 47.5 cm long, 2.54 cm wide, and 0.635 cm thick. A two-sided notch with a length of 5.5 cm is created in the specimen by milling 0.125 cm in thickness from both top and bottom surfaces.

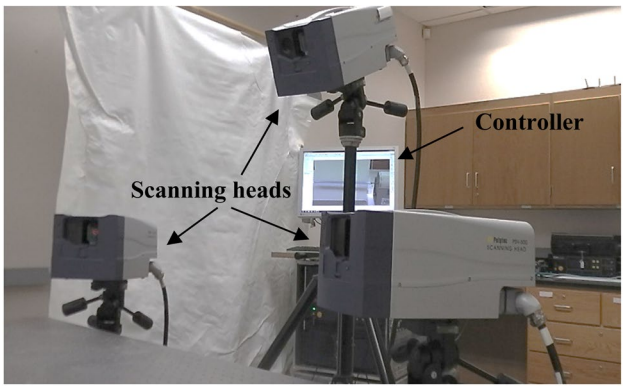

Fig. 13 3D SLV with three scanning heads and a controller

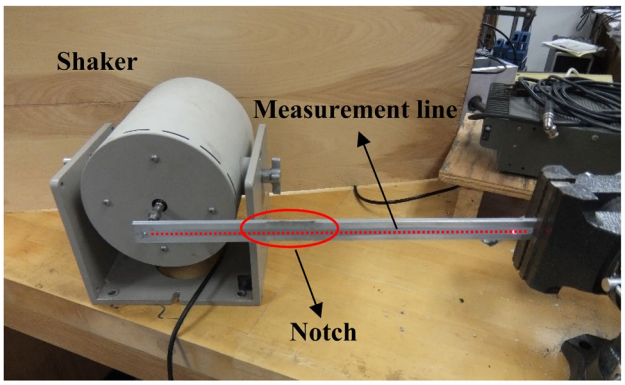

(a)

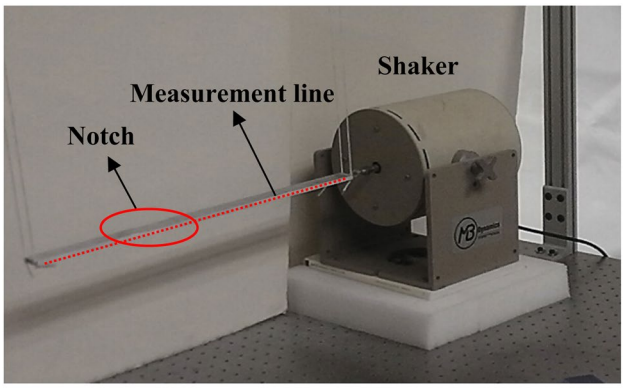

(b)

Fig. 14 Aluminum beam with a two-sided notch, which is excited by an electromagnetic shaker in **a** transverse and **b** axial directions, respectively

To excite flexural vibration of the beam, it is clamped at one end and an MB Dynamics Modal 50A electromagnetic shaker is attached to it at a distance of 1.3 cm away from the free end, as shown in Fig. 14a. The distance between the clamped and free ends of the beam is 45.2 cm. In this case, the measurement line (indicated by dots in Fig. 14a to represent the laser spot moving along it) along one milled side of the beam is 41.15 cm in length, whose origin is 2.25 cm away from the clamped end; the notch is 22.8 to 28.3 cm away from the origin of the measurement line. The beam is excited by harmonic excitation generated by the shaker in the transverse direction. Excitation frequencies are selected to be the fifth flexural natural frequency of the beam at 1224.4 Hz and frequency of 1200 Hz that is close to it. Steady-state velocity responses of the beam are acquired by the 3D SLV from 255 uniformly distributed measurement points along the measurement line. Flexural operating deflection shapes (ODSs) are extracted using LMS Test.Lab 9b's animation module by analyzing averaged cross-power spectra of the measurement points. The real part of the ODS at the fifth natural frequency of 1224.4 Hz approximates the fifth undamped MS of this lightly damped beam, since its magnitude is much larger than that of the imaginary part, which leads to a higher SNR [7] that benefits structural damage detection. Similarly, the real part of the ODS at 1200 Hz is regarded as the corresponding undamped flexural SRSHE.

To excite longitudinal vibration of the beam, it is suspended by four flexible strings that are glued to its four corners of the upper surface; the electromagnetic shaker is attached to the end farther away from the notch, as shown in Fig. 14b. In this case, the measurement line (indicated by dots in Fig. 14b to represent the laser spot moving along it) along one unmilled side of the beam is 45 cm in length, whose origin is 2.3 cm away from the excitation location; the notch is 25 to 30.5 cm away from the origin of the measurement line. As the maximum excitation frequency of the shaker is 5000 Hz, and the first undamped longitudinal natural frequency of the beam is estimated to be 4968.6 Hz by the analytical solution in Sect. 4, the first longitudinal mode of the beam cannot be accurately acquired due to the limitation of the shaker. The shaker produces a harmonic force at 4900 Hz, which is close to the first undamped longitudinal natural frequency of the beam and within the excitation frequency range of the shaker, to excite the beam in the axial direction. Steady-state velocity responses of the beam are acquired by the 3D SLV from 255 uniformly distributed measurement points along the measurement line. The real part of the ODS at 4900 Hz is regarded as the longitudinal SRSHE for this lightly-damped beam. Consequently, only the longitudinal SRSHE is used in this section to validate the capability of MSVSs for damage detection of the beam.

5.2 Experimental Results

5.2.1 Damage Detection Using MCVSs

In the flexural vibration case of the damaged beam, Fig. 15a shows its fifth MS at 1224.24 Hz and Fig. 15b shows its flexural SRSHE at 1200 Hz. By Eq. (5), CVSs for the flexural MS and SRSHE are obtained and shown in Fig. 16a and b, respectively. It can be seen from Fig. 16 that noise interference is evident, leading to only one discontinuity in either CVS that corresponds to the right edge of the notch and a fake discontinuity in the undamaged region. To eliminate noise interference, MCVSs for the flexural MS and SRSHE are obtained by Eq. (23) and shown in Figs. 17a

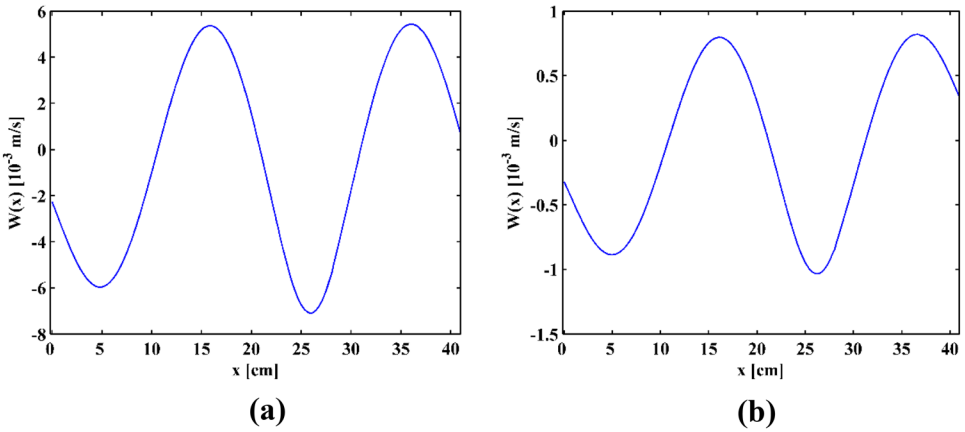

Fig. 15 Flexural **a** MS at 1224.4 Hz and **b** SRSHE at 1200 Hz

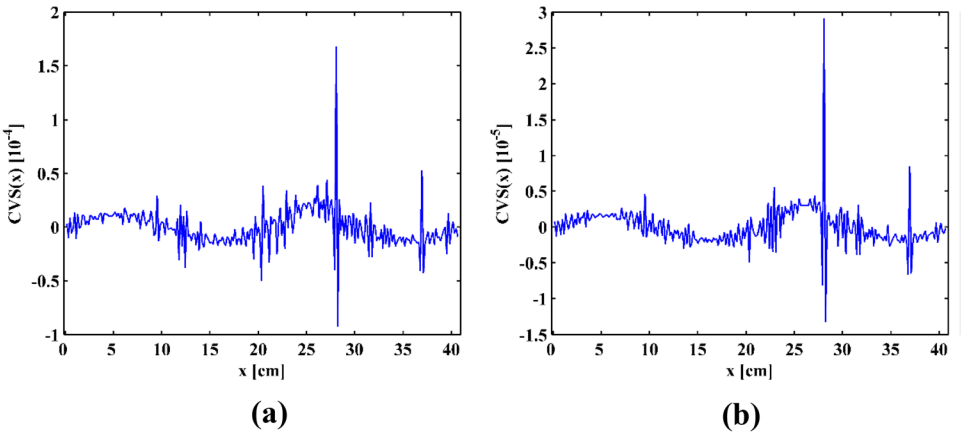

Fig. 16 CVSs for the flexural **a** MS at 1224.4 Hz and **b** SRSHE at 1200 Hz

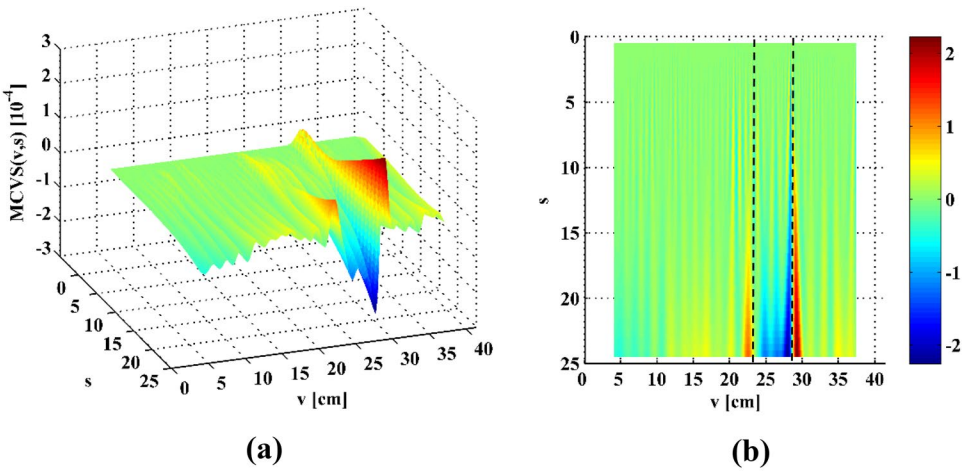

Fig. 17 **a** MCVS for the flexural MS at 1224.4 Hz and **b** its top view

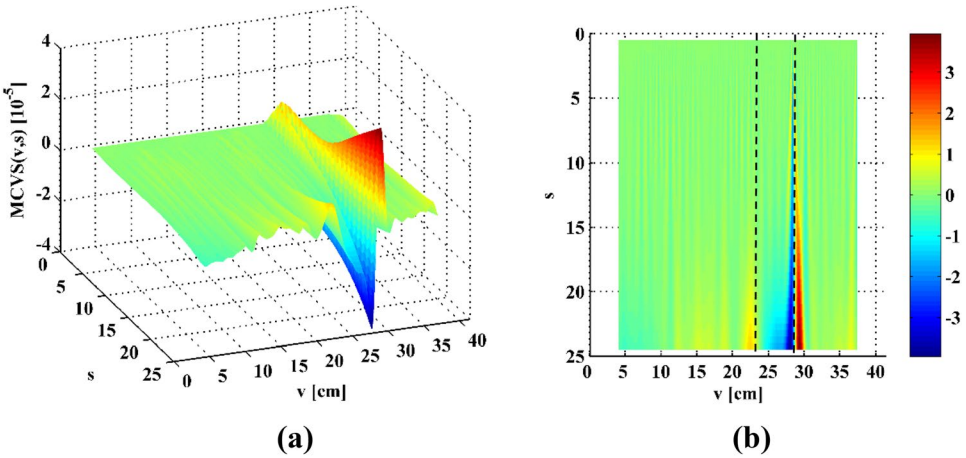

Fig. 18 **a** MCVS for the flexural SRSHE at 1200 Hz and **b** its top view

and 18a, respectively. In either figure, amplitudes of two pairs of singularity peaks and valleys that increase with the scale parameter s indicate locations of the two edges of the notch; the second peak is clear, whereas the first one is less pronounced but sufficiently clear for damage identification, because the first edge of the notch is close to one of nodes of the corresponding flexural MS and SRSHE of the beam, where the small vibration amplitudes lead to low SNRs. Consequently, the damage-induced discontinuities can be masked by noise interference. The damage location can be determined in top views of the MCVSs as shown in Figs. 17b and 18b, which spans from about $x = 22.8$ to 28.3 cm. The detected notch location corresponds to the actual location of the notch indicated by two dashed lines.

5.2.2 Damage Detection Using MSVSs

In the longitudinal vibration case of the damaged beam, Fig. 19a shows the longitudinal SRSHE at 4900 Hz, from which the SVS is obtained by Eq. (10) and shown in Fig. 19b. It can be seen from Fig. 19b that damage-induced discontinuities in the SVS are masked by noise interference. The MSVS is obtained by Eq. (24) and shown in Fig. 20a, where amplitudes of two pairs of singularity peaks and valleys that increase with the scale parameter s clearly indicate occurrence of the damage. In the top view of the MSVS shown in Fig. 20b, edges that lie in the middle of the peaks and valleys pinpoint the notch that spans from about $x = 25$ to 30.5 cm, which is in good agreement with the actual location of the notch indicated by two dashed lines.

6 Comparison and Conclusions

Structural damage detection methods relying on laser-measured VSs have become a research focus in the past decade. In this comparative study, structural damage detection methods using derivatives of laser-measured flexural and longitudinal VSs of a beam/bar are compared and discussed in aspects of physical senses, analytical formulation, and numerical evaluation. The following conclusions can be drawn from their comparison:

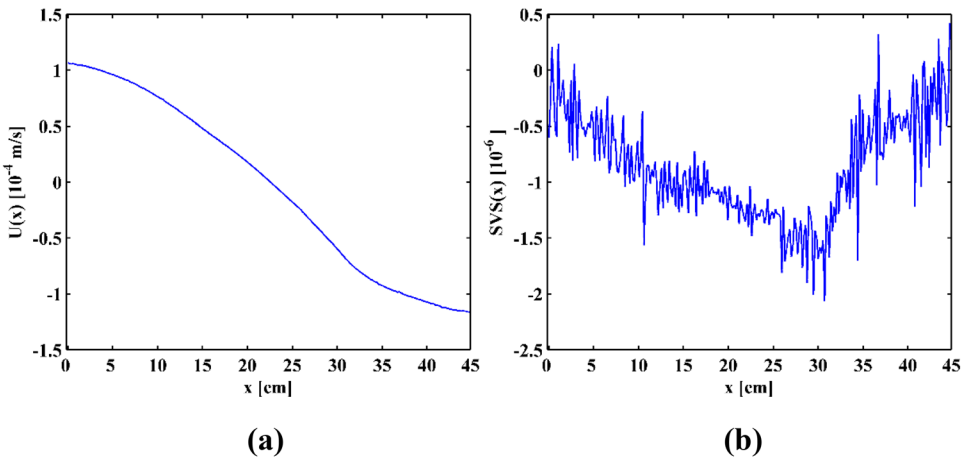

Fig. 19 **a** Longitudinal SRSHE at 4900 Hz and **b** its SVS

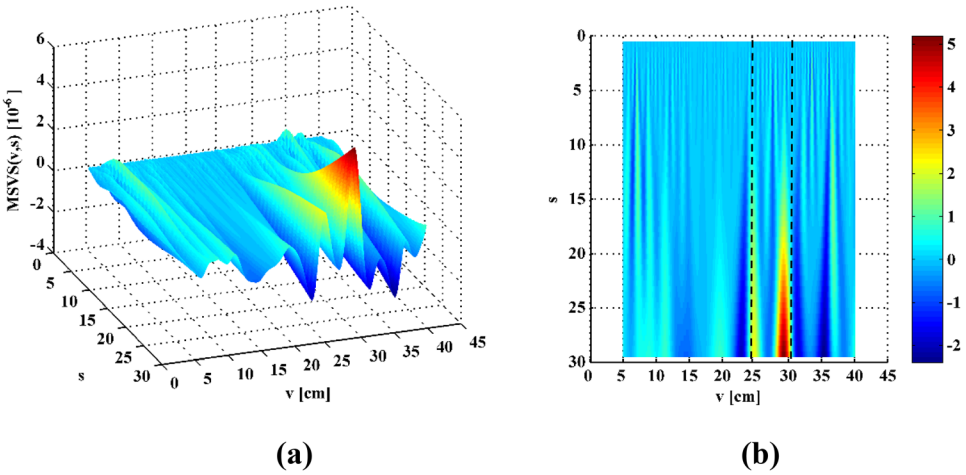

Fig. 20 **a** MSVS for the longitudinal SRSHE at 4900 Hz and **b** its top view

(1) Physical senses of damage detection principles using CVSs and SVSs for respective flexural and longitudinal VSs are distinct: damage such as a notch with reduced cross-sectional dimensions can cause changes in both bending and axial stiffnesses. For flexural vibration, due to the damage-caused change in the bending stiffness, the second-order derivatives of flexural VSs, i.e., CVSs, become discontinuous at damage edges to balance continuity conditions of bending moments, whereby damage can be indicated and located by discontinuities in CVSs. For longitudinal vibration, due to the damage-caused change in the axial stiffness, the first-order derivatives of longitudinal VSs, i.e., SVSs, become discontinuous at damage edges to balance continuity conditions of axial forces, whereby damage can be indicated and located by discontinuities in SVSs. Analytical formulation of VSs in Sect. 4 is in accord with the physical senses of the CVSs and SVSs in damage detection.

(2) Although derivatives of both flexural and longitudinal VSs can be used to detect damage in a beam/bar, compared with flexural VSs commonly used for structural damage detection, it is much more difficult to excite and measure its longitudinal vibration. Longitudinal modes have much higher natural frequencies than flexural modes. Although it is difficult to acquire longitudinal vibration, longitudinal VSs can be useful for detecting damage in such a structure as a cable, since flexural vibration of a cable is mainly governed by its tension in it and not its bending stiffness. In these cases, SVSs instead of CVSs are suitable to detect damage that causes reduction in elastic modulus and cross-sectional dimensions. Analytical and experimental validation show that compared with commonly used derivatives of flexural VSs, derivatives of longitudinal VSs have the same capability in detecting damage in a beam/bar.

(3) The common deficiency of CVSs and SVSs is their susceptibility to environmental noise interference because differential operations can largely amplify noise components involved in laser-measured VSs with dense sampling. In this study, a scheme of integrating the WT-based multiscale analysis into the CVSs and SVSs is proposed, by which new concepts of MCVS and MSVS are formulated, respectively. The MCVSs and MSVSs are capable of enhancing the robustness of the CVSs and SVSs against noise interference. By gradually increasing scale parameters to satisficing levels, noise components in the MCVSs and MSVSs can be gradually eliminated while damage-induced discontinuities can be retained for structural damage detection.

Acknowledgements Weidong Zhu and Yongfeng Xu are grateful for the financial support from the National Science Foundation through Grant Nos. CMMI-1763024 and CMMI-1762917, respectively. Wei Xu is grateful for the support from the National Natural Science Foundation of China through Grant No. U1765204. The authors are also thankful for the help on the experiment from Scott Smith in the Department of Mechanical Engineering at the University of Maryland, Baltimore County.

References

1. Farrar, C., Worden, K.: An introduction to structural health monitoring. Philos. Trans. R. Soc. A **365**, 303–315 (2007)
2. Xu, Y., Zhu, W.: Non-model-based damage identification of plates using measured mode shapes. Struct. Health Monit. **16**, 3–23 (2017)
3. Xu, Y., Zhu, W., Smith, S.: Non-model-based damage identification of plates using principal, mean and Gaussian curvature mode shapes. J. Sound Vib. **400**, 626–659 (2017)
4. Chen, D., Xu, Y., Zhu, W.: Experimental investigation of notch-type damage identification with a curvature-based method by using a continuously scanning laser Doppler vibrometer system. J. Nondestr. Eval. **36**, 38 (2017)

5. Chen, D., Xu, Y., Zhu, W.: Identification of damage in plates using full-field measurement with a continuously scanning laser Doppler vibrometer system. J. Sound Vib. **422**, 542–567 (2018)
6. Chen, D., Xu, Y., Zhu, W.: Non-model-based identification of delamination in laminated composite plates using a continuously scanning laser Doppler vibrometer system. J. Vibrat. Acoust. **140**, 041001 (2018)
7. Xu, W., Zhu, W., Smith, S., Cao, M.S.: Structural damage detection using slopes of longitudinal vibration shapes. J. Vib. Acoust. **138**, 345013 (2016)
8. Pandey, A., Biswas, M., Samman, M.: Damage detection from changes in curvature mode shapes. J. Sound Vib. **145**, 321–332 (1991)
9. Cao, M., Qiao, P.: Novel Laplacian scheme and multiresolution modal curvatures for structural damage identification. Mech. Syst. Signal Process. **23**, 1223–1242 (2009)
10. Yoon, M., Heider, D., Gillespie Jr., J., Ratcliffe, C., Crane, R.: Local damage detection with the global fitting method using mode shape data in notched beams. J. Nondestr. Eval. **28**, 63–74 (2009)
11. Yoon, M., Heider, D., Gillespie Jr., J., Ratcliffe, C., Crane, R.: Local damage detection with the global fitting method using operating deflection shape data. J. Nondestr. Eval. **29**, 25–37 (2010)
12. Kim, J., Lee, E., Rahmatalla, S., Eun, H.: Non-baseline damage detection based on the deviation of displacement mode shape data. J. Nondestr. Eval. **32**, 14–24 (2013)
13. Cao, M., Xu, W., Ostachowicz, W., Su, Z.: Damage identification for beams in noisy conditions based on Teager energy operator-wavelet transform modal curvature. J. Sound Vib. **333**, 1543–1553 (2014)
14. Xu, Y., Zhu, W., Liu, J., Shao, Y.: Identification of embedded horizontal cracks in beams using measured mode shapes. J. Sound Vib. **333**, 6273–6294 (2014)
15. Cao, S., Ouyang, H.: Robust structural damage detection and localization based on joint approximate diagonalization technique in frequency domain. Smart Mater. Struct. **26**, 015005 (2017)
16. Yang, Z., Radzienski, M., Kudela, P., Ostachowicz, W.: Fourier spectral-based modal curvature analysis and its application to damage detection in beams. Mech. Syst. Signal Process. **84**, 763–781 (2017)
17. Qiao, P., Lestari, W., Shah, M.G., Wang, J.: Dynamics-based damage detection of composite laminated beams using contact and noncontact measurement systems. J. Compos. Mater. **41**, 1217–1252 (2007)
18. Sazonov, E., Klinkhachorn, P.: Optimal spatial sampling interval for damage detection by curvature or strain energy mode shapes. J. Sound Vib. **285**, 783–801 (2005)
19. Shi, Z., Law, S., Zhang, L.: Structural damage detection from modal strain energy change. J. Eng. Mech. **126**, 1216–1223 (2000)
20. Cao, M., Cheng, L., Su, Z., Xu, H.: A multi-scale pseudo-force model in wavelet domain for identification of damage in structural components. Mech. Syst. Signal Process. **28**, 638–659 (2012)
21. Cao, M., Su, Z., Cheng, L., Xu, H.: A multi-scale pseudo-force model for characterization of damage in beam components with unknown material and structural parameters. J. Sound Vib. **332**, 5566–5583 (2013)
22. Xu, H., Su, Z., Cheng, L., Guyader, J., Hamelin, P.: Reconstructing interfacial force distribution for identification of multi-debonding in steel-reinforced concrete structures using noncontact laser vibrometry. Struct. Health Monit. **12**, 507–521 (2013)
23. Liew, K., Wang, Q.: Application of wavelet theory for crack identification in structures. J. Eng. Mech. **124**, 152–157 (1998)
24. Wang, Q., Deng, X.: Damage detection with spatial wavelets. Int. J. Solids Struct. **36**, 3443–3468 (1999)
25. Rucka, M., Wilde, K.: Application of continuous wavelet transform in vibration based damage detection method for beams and plates. J. Sound Vib. **297**, 536–550 (2006)
26. Kim, H., Melhem, H.: Damage detection of structures by wavelet analysis. Eng. Struct. **26**, 347–362 (2004)
27. Pawar, P., Ganguli, R.: Modeling multi-layer matrix cracking in thin walled composite rotor blades. Journal of the American Helicopter Society **50**, 354–366 (2005)
28. Weaver, W., Timoshenko, S., Young, D.: Vibration Problems in Engineering. Wiley, New York (1990)
29. Mallat, S.: A Wavelet Tour of Signal Processing. Academic Press, New York (2008)
30. Leissa, A., Qatu, M.: Vibration of Continuous Systems. McGraw Hill, New York (2011)

Publisher's Note Springer Nature remains neutral with regard to jurisdictional claims in published maps and institutional affiliations.